

Design Principles for Efficient Singlet Fission in Anthracene-based Organic Semiconductors

Youn Jue Bae,^a Joseph A. Christensen,^a Gyeongwon Kang,^a Christos D Malliakas,^a Jiawang Zhou,^a Jordan N. Nelson,^a Ryan M. Young,^a Yi-Lin Wu,^{a,b} Richard P. Van Duyne,^a George C. Schatz,^a and Michael R. Wasielewski^{*a}

^a Department of Chemistry and Institute for Sustainability and Energy at Northwestern, Northwestern University, Evanston IL 60208-3113

^bSchool of Chemistry, Cardiff University, Main Building, Park Place, Cardiff CF10 3AT, UK

ABSTRACT

Singlet fission (SF) in two or more electronically coupled organic chromophores converts a high-energy singlet exciton into two low-energy triplet excitons, which can be used to increase solar cell efficiency. Many known SF chromophores are unsuitable for device applications due to chemical instability and low triplet state energies. This work summarizes structurally dependent SF dynamics for 9,10-bis(phenylethynyl)anthracene (BPEA) and its derivatives in the solid-state using time-resolved optical spectroscopies, and electronic structure calculations. By modulating the packing structure in thin films, we can effectively tune electronic energy and coupling. The systematic study in BPEA organic semiconductors shows that maximizing the thermodynamic driving force can achieve the highest SF rate and efficiency.

Keywords: Singlet Fission, Organic Semiconductors, Frankel Excitons, Anthracene

1. INTRODUCTION

Singlet fission (SF) is a multiple exciton generation process in organic semiconductors where a singlet exciton, generated via photon absorption, energetically down-converts into two triplet excitons.[1] Over the past decade, SF chromophores have attracted renewed attention because of their ability to overcome the Shockley–Quiesser limit on the theoretical efficiency of single-junction solar cells by mitigating thermalization losses.[2] Specifically, down-converted low energy triplet excitons can be harvested by either energy transfer or charge transfer to single junction solar cells, which then increases the closed-circuit current.[3] Previous studies have demonstrated Dexter type energy transfer from two triplet excitons in tetracene and pentacene to lead-based quantum dots.[4, 5] Charge transfer from the triplet exciton is also possible if the SF chromophores are paired with a suitable electron acceptor or donor; for example, a solar cell using pentacene coupled with C₆₀ achieved an external quantum efficiency of 133 %. [6] Recently, triplet exciton transfer from tetracene to a silicon single junction cell has been demonstrated, where of the 133% exciton transfer from the tetracene layer to Si, 56 % comes from singlet excitons and 76 % from triplet excitons.[7] Such competition between singlet and triplet exciton transfer exists as a result of the slow SF rate in tetracene. Thus, it is crucial to discover SF materials that have high triplet energies, ideally greater than a band gap of 1.1- 1.3 eV, with fast SF rates.

Although anthracene has been demonstrated to undergo SF,[8] SF is only viable from higher lying singlet excited state because of its high triplet energy (1.8 eV). In anthracene crystals, SF is competitive with internal conversion and thus SF efficiency is extremely low (3%). However, functionalization of anthracene with phenylethynyl groups at 9,10 positions to form BPEA achieves better energetics for SF. This modification lowers the triplet energy to ~1.20 eV while maintaining the singlet energy at ~ 2.40 eV. In addition, BPEA is a robust, industrial dye with excellent thermal and photostability and chemical modularity. In this presentation, we summarize the structurally dependent SF dynamics of BPEA and its derivatives in the solid-state using time-resolved optical spectroscopies, and electronic structure calculations. We systematically control molecular packing by changing the composition of polymorphs and adding functional groups at the *para* position of the phenyls. Such changes in molecular structure result in different packing, ultimately modulating both the electronic coupling and thermodynamic driving force.

2. EXPERIMENTAL METHODS

2.1 Materials and film preparation

BPEA was purchased from Sigma Aldrich. Synthetic procedures for preparing BPEA derivatives have been reported elsewhere.[9] ~100 nm films of BPEA and its derivatives were prepared on sapphire substrates at room temperature at a rate of 0.2 Å/s in a vacuum thermal evaporator (Denton Vacuum DV502-A).

2.2 Instrumentation

Steady-state optical absorption spectra of the film samples were measured using a Shimadzu UV-3600 UV/Vis/NIR spectrometer equipped with an integrating sphere. Steady-state fluorescence spectra of film samples were measured in the right-angle mode with a HORIBA Nanolog spectrophotometer equipped with an integrating sphere (Horiba Quanta - ϕ) to determine absolute fluorescence quantum yields. Femtosecond transient absorption (fsTA) experiments on the thin films were performed using 14 nJ, 414 nm, 100 fs excitation pulses generated by a 100 kHz repetition rate laser system to obtain SF dynamics. The data were analyzed using global kinetic analysis, as described in detail previously.[10] Nanosecond transient absorption (nsTA) experiments were performed using a 1.0 mJ, 414 nm, 7 ns excitation pulse generated by 10 Hz repetition rate laser system[11] to obtain the triplet yield.

2.3 Computational Details

The electronic couplings were calculated from the integral matrix elements using the density functional theory (DFT) with the Amsterdam Density Functional (ADF) package.[12] The effective coupling between orbitals i and f, V_{if} , was calculated using the following equation:[13]

$$V_{if} = \frac{J_{if} - \frac{1}{2}S_{if}(e_i + e_f)}{1 - S_{if}^2} \quad (1)$$

where J_{if} is the Fock matrix element between a pair of monomers, S_{if} is the overlap integral, e_i and e_f are the Fock matrix elements within a monomer.

Singlet and triplet excitation energies, $E(S_1)$ and $E(T_1)$, were calculated using the time-dependent density functional theory (TDDFT) with the ADF package. $E(T_1 T_1)$ was obtained by doubling $E(T_1)$. The CT state energy, $E(CT)$, was calculated using a Weller-like equation:

$$E(CT) = IP + EA + E_{elec} + E_{ind} \quad (2)$$

Here, ionization energy (IP) and electron affinity (EA) of monomer were obtained from DFT, whereas the induction (E_{ind}) and electrostatic (E_{elec}) energies were determined using the classical the Direct Reaction Field (DRF) method[14] suggested by Mirjani *et al.* Atomic charges of both neutral and charged dimers for DRF calculations were obtained from Mulliken population analysis using DFT.

Considering the first-order coupling of CT states to the initially excited singlet state, S_1 , and the final triplet state, $(T_1 T_1)$, the effective electronic coupling for the superexchange mechanism,[15] $J_{SE,eff}$, was calculated using the Eq. 3:

$$J_{SE,eff} = < S_1 S_0^1 | \hat{V} | T_1 T_1^1 > = < S_1 S_0^0 | \hat{H}_{el} | T_1 T_1^0 > - \frac{2(V_{LL} V_{LH} - V_{HH} V_{HL})}{[E(CT) - E(TT)] + [E(CT) - E(S_1)]} \quad (3)$$

The first term on the right-hand side of the equation will be ignored since the direct two-electron coupling is small compared to the four 1-electron coupling. V_{LL} and V_{HH} are the 1-electron coupling of the LUMO and HOMO of the two molecules, respectively, whereas V_{LH} and V_{HL} are the electronic couplings between the LUMO of the first molecule and the HOMO of the second molecule, and vice versa.

3. RESULTS/ DISCUSSION

Films **1** and **2** are prepared by thermal vapor deposition of BPEA, followed by solvent vapor (CH_2Cl_2) annealing for film **1** and thermal annealing at 120 °C for film **2**. Films **3**, **4** and **5** are prepared by thermal vapor deposition of 4,4'-difluoro-BPEA, 4-fluoro-4'-methoxy-BPEA and 4,4'-dimethoxy-BPEA, respectively, followed by solvent vapor (CH_2Cl_2) annealing. The powder X-ray pattern (PXRD) of the polycrystalline powder scraped off vapor deposited films on the sapphire substrate is compared to the simulated PXRD from the single crystal structure (Figure 1).

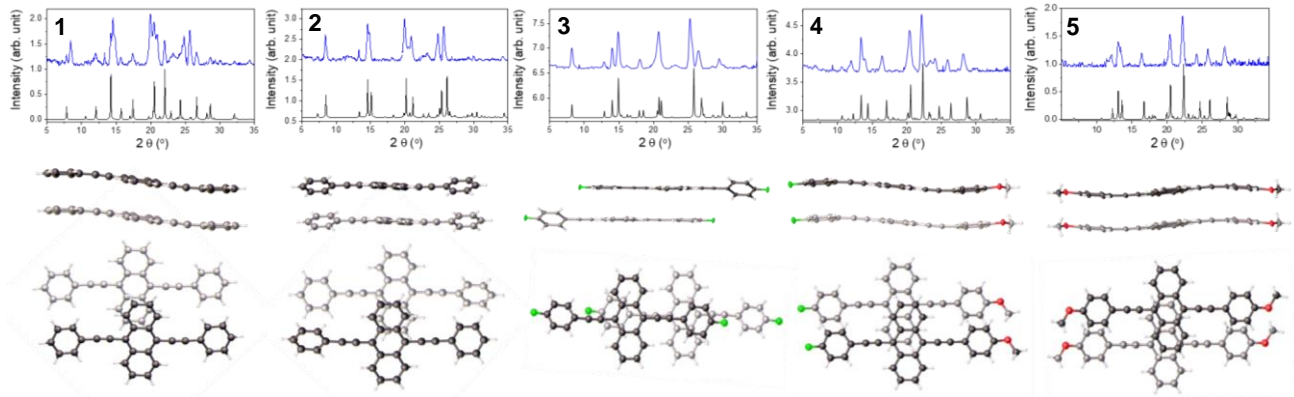


Figure 1. Comparison of the simulated PXRD pattern from a single crystal (black) and PXRD of the polycrystalline powder scraped off a vapor-deposited/annealed films (blue) of **1-5** with the respective nearest dimer unit within the crystal structure. In the crystal structure, green atoms are fluorine, red are oxygen, white are hydrogen and grey are carbon.

All but film **1**, which is composed of two different polymorphs (*C*2/*c* and *Pbcn* space groups), have only a single polymorph. The composition of *C*2/*c* and *Pbcn* polymorph in film **1** is determined to be $61.2 \pm 0.5\%$ and $38.8 \pm 0.5\%$, respectively, using Rietveld fitting.[9] Since *C*2/*c* polymorph is the major composition in film **1**, the dimer unit in Figure 1 shows *C*2/*c* packing structure. All films are highly crystalline based on the peak sharpness compared to other SF thin films of rylene[11, 16] and acene derivatives.[17]

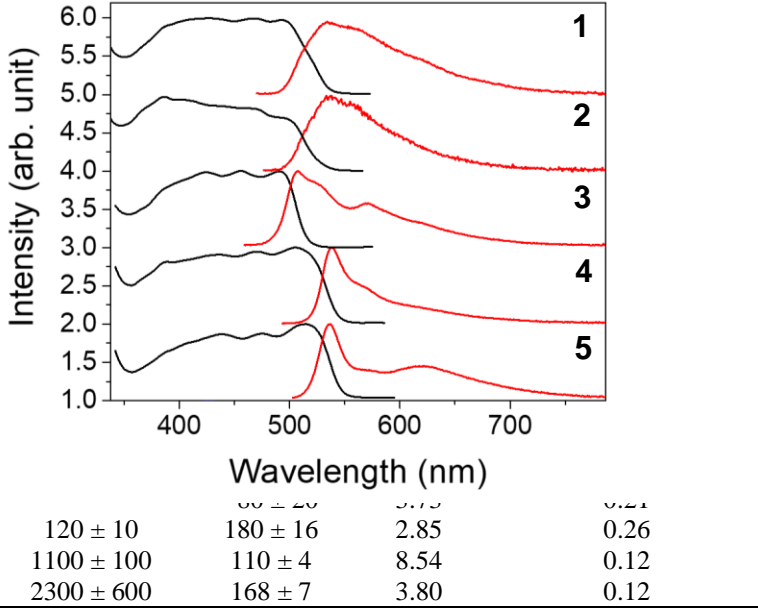
The difference in packing structure of each film is highlighted in the dimer from the crystal structure (Figure 1). The chromophore packing within the crystal structures of **1-5** is analyzed by extracting the nearest dimer unit within the crystal structure. The $\pi-\pi$, lateral slip and longitudinal slip distances are shown in Table 1.

Table 1. $\pi-\pi$, lateral and longitudinal slip distances of the nearest dimer unit within the crystal structures BPEA (**1-2**) and its derivatives (**3-5**).

Films	$\pi-\pi$ (Å)	Lateral slip distance (Å)	Longitudinal slip distance (Å)
1	3.40	4.06	0.800
2	3.45	3.34	0.800
3	3.35	0.367	7.280
4	3.41	3.93	0.345
5	3.42	3.87	0.336

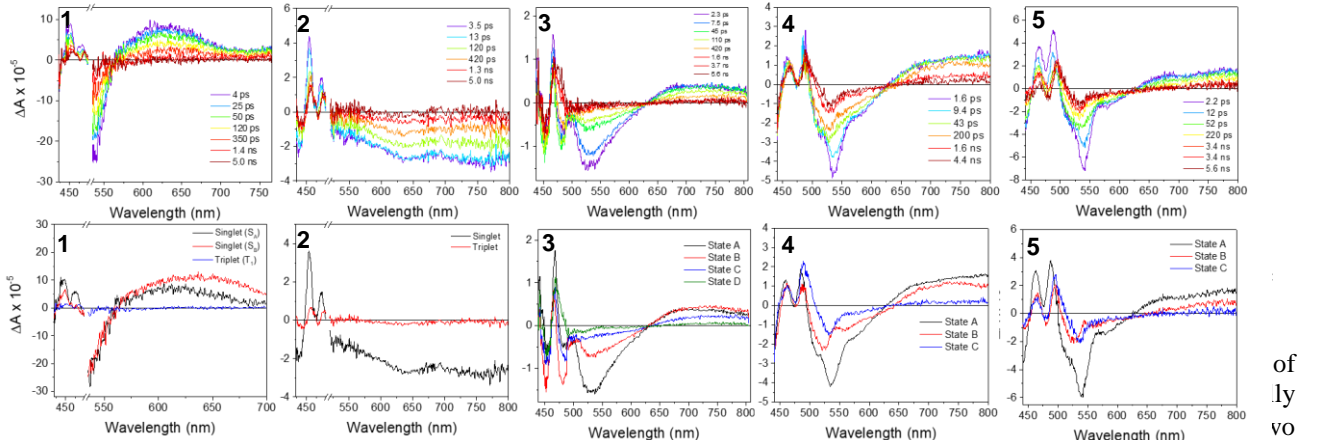
All of the dimer units have $\pi-\pi$ distance close to 3.40 Å. Films **1** and **2** have the same longitudinal slip distance (0.8 Å) but different lateral slip distances. Film **3** has a large longitudinal slip distance (7.28 Å) but almost no lateral slip, while **4** and **5** have significant lateral slip distances of 3.93 Å and 3.87 Å, respectively, and almost no longitudinal slip. Films **4** and **5** have shorter longitudinal slip distances compared to films **1** and **2**.

Steady state absorbance and emission spectra of the films were measured (Figure 2) to obtain the first excited singlet energy, $E(S_1)$. Among the five films, film **3** has the highest $E(S_1)$ of 2.48 eV followed by **1** (2.43 eV), **2** (2.43 eV), **4** (2.34 eV), and **5** (2.34 eV). The large dihedral angle in film **3** decreases the electronic conjugation between the anthracene core and the phenyl group, which leads to a higher $E(S_1)$. The triplet energies of the thin films were estimated using triplet energy transfer from palladium octabutoxyphthalocyanine (PdPc) and to singlet oxygen. The estimated triplet energy is 0.98 – 1.24 eV, where the lower limit comes from singlet oxygen and the upper limit from PdPc.[18] Since triplet excitons are more localized than singlet excitons, triplet energies are assumed to be constant amongst the films. Hence, the triplet energy is approximated between 0.98 eV and 1.24 eV. With these assumptions, the thermodynamic driving force for SF is calculated to be the difference between $E(S_1)$ and $E(T_1T_1 = 1.11$ eV). Film **3** has the greatest thermodynamic driving force of 0.26 eV followed by **1**, **2**, **4** and **5** (Table 2).



^a $E(T_1 T_1)$ is approximated to be 1.11 eV which is a mean value between 0.98 and 1.24 eV.

In order to examine the SF dynamics, low-fluence fsTA spectroscopy was used with excitation densities of (1.0×10^{17} excitons·cm⁻³). It is crucial that the excited state be studied in the low excitation regime to minimize singlet-singlet annihilation. From the fsTA spectra, we observe ground-state bleaching (GSB), stimulated emission (SE) and singlet excited-state absorption (ESA) at early times; at later times, triplet formation is observed around 450-550 nm (Figure 3).



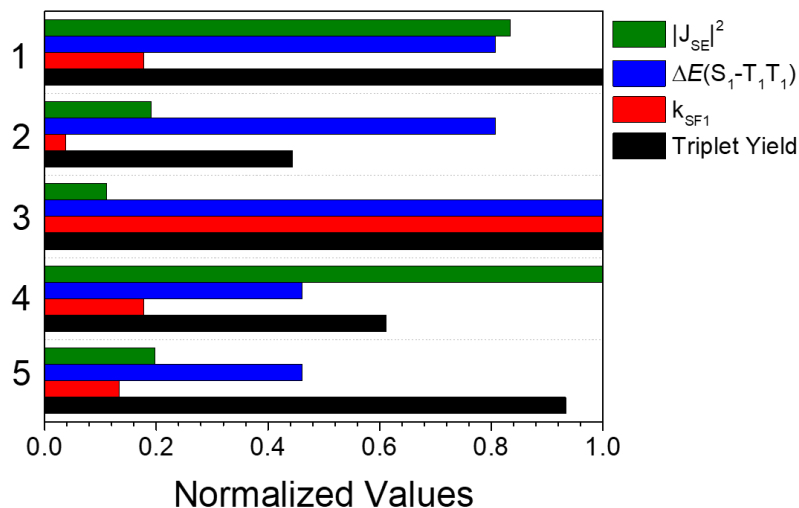
different polymorphs, is globally fitted using the two parallel processes of $A \rightarrow B \rightarrow GS$, where two singlet populations originate from two different polymorphs. From the kinetic fitting, the SF rate of $C2/c$ polymorph is $(90 \pm 30 \text{ ps})^{-1}$ and that of $Pbcn$ is $(430 \pm 30 \text{ ps})^{-1}$.

The BPEA derivatives differ from the parent BPEA films in that the derivatives require more than one singlet excited population, which is attributed to heterogeneity in the film and small degree of excimer formation. Since the excited states are not purely singlet, excimer, or triplet, we use evolution-associated fitting, where each state has mixture of singlet, excimer and/or triplet, similar to that observed in terrylenediimide systems.[19, 20] Film **3** is globally fitted using $A \rightarrow B \rightarrow C \rightarrow D \rightarrow GS$. Based on the increase in GSB feature in state B and C (Figure 2), τ_A and τ_B are assigned to SF. Although there is a single polymorph in the thin film of **1**, if some degree of heterogeneity exists in terms of grain size and crystallinity, this could form local hot spots where SF is more favorable, as seen in pentacene[21] and terrylenediimide films[16]. Both films of **4** and **5** are globally fitted using $A \rightarrow B \rightarrow C \rightarrow GS$. There are distinct spectral changes between state A and B in the film of **5**, where state B resembles the triplet feature. States A in the film **4** has

similar spectral features to state B; however, state B has increased red-shifted stimulated emission features. Presumably, state B in the film of **4** has more triplet population than in film **5**. Overall, the BPEA derivatives have more distributed kinetics compared to BPEA films.

nsTA spectra of the films were employed to determine their triplet yields using the singlet depletion method, which is independent of the choice of kinetic model. This method is particularly useful in estimating triplet yields for systems with overlapping GSB and triplet ESA features. The number of excited molecules were calculated from the excitation pulse energy, laser spot size, and film thickness to obtain the expected GSB spectrum; then, the number of triplet states was estimated by adding the scaled ground-state bleach to the excited state triplet nsTA spectrum. Based on this analysis, films of **1** and **3** have the highest triplet yield of 180 % followed by the films of **5** (168 %), **4** (110 %), and **2** (80%).

Electronic coupling, J_{SE} , is an important factor controlling SF rate and efficiency.[1] We calculated J_{SE} using the dimer model, assuming the mechanism of SF is superexchange. The film of **4** has the highest electronic coupling of 8.54 meV, followed by that of **1** (7.80 meV), **5** (3.80 meV), **2** (3.73 meV) and **3** (2.85 meV). We find strong correlation between electronic coupling and τ_{SF1} in all films except that of **3** (Figure 4).



between films **1** and **2**, where the SF rate for $C2/c$ is estimated to be 4.4 times faster than that of $Pbcn$, matching the experimental rate ratio of 4.5 ± 0.2 .

Now, correlating the triplet yield to the SF rate, electronic coupling and thermodynamic driving force, we find that the triplet yield is most strongly correlated to thermodynamic driving force. For instance, although film **3** has the lowest $|J_{SE}|^2$, it undergoes the fastest SF with the highest triplet yield, attributed to the greatest thermodynamic driving force. Following the film of **3**, films of **1** and **2** have greater thermodynamic driving forces than films of **4** and **5**. The film of **1** has both greater thermodynamic driving force and electronic coupling compared to films of **2**, **4**, and **5** and thus, undergoes faster SF with greater triplet yield; however, film **2** which has greater thermodynamic driving force undergoes slower and less efficient SF than films of **4** and **5**. One possible reason is that the crystal structure of the film of **2** enhances fluorescence emission, resulting in the highest fluorescence quantum yield of 30%, meaning that only 70% of the singlet excitons can undergo SF. Between films of **4** and **5**, which have the same thermodynamic driving force, film **4**, which has greater electronic coupling, undergoes less efficient SF. This is because the molecule has push-pull character which results in a low calculated CT energy. Such low CT energy presumably introduces excimer trap states as evidenced in significantly more red-shifted emission spectra and low triplet yield compared to all the other films.

4. CONCLUSION

We studied five different thin film made of BPEA and its derivatives. We can tune the composition of different polymorphs of BPEA in the film by changing the annealing method. Different packing structures in films of **3-5** result from adding functional groups at the *para* positions of the phenyls in BPEA. Among all the structurally different films studied here, triplet yield increases with increasing thermodynamic force. The film **3**, which has the greatest driving force, undergoes fastest SF with the highest triplet yield, followed by the films of **2** and **5**. The simple dimer model used here to calculate the effective electronic coupling predicts the rate of SF relatively well. The film **3** has the strongest potential to be used as a solar cell device because of its fast 17 ps SF time and its high 180% triplet yield.

5. ACKNOWLEDGEMENT

This work was supported by the U.S. Department of Energy, Office of Science, Office of Basic Energy Sciences under Award DE-FG02-99ER14999 (M.R.W.). G.K., R.P.V.D., and G.C.S. acknowledge support from the Air Force Office of Scientific Research MURI (FA9550-14-1-0003). GK and GCS (theory work) acknowledge the LEAP Center, DOE grant DE-SC0001059. Y.B. thanks Phi Lamda Upsilon and Northwestern University for travel grant.

REFERENCES

- [1] M. B. Smith, and J. Michl, “Recent Advances in Singlet Fission,” *Ann. Rev. Phys. Chem.*, 64(1), 361-386 (2013).
- [2] M. C. Hanna, and A. J. Nozik, “Solar conversion efficiency of photovoltaic and photoelectrolysis cells with carrier multiplication absorbers,” *J. Appl. Phys.*, 100(7), 074510 (2006).
- [3] A. Rao, and R. H. Friend, “Harnessing singlet exciton fission to break the Shockley–Queisser limit,” *Nature Reviews Materials*, 2, 17063 (2017).
- [4] N. J. Thompson, M. W. B. Wilson, D. N. Congreve *et al.*, “Energy harvesting of non-emissive triplet excitons in tetracene by emissive PbS nanocrystals,” *Nature Materials*, 13, 1039 (2014).
- [5] M. Tabachnyk, B. Ehrler, S. Gélinas *et al.*, “Resonant energy transfer of triplet excitons from pentacene to PbSe nanocrystals,” *Nature Materials*, 13, 1033 (2014).
- [6] D. N. Congreve, J. Lee, N. J. Thompson *et al.*, “External Quantum Efficiency Above 100% in a Singlet-Exciton-Fission-Based Organic Photovoltaic Cell,” *Science*, 340(6130), 334 (2013).
- [7] M. Einzinger, T. Wu, J. F. Kompalla *et al.*, “Sensitization of silicon by singlet exciton fission in tetracene,” *Nature*, 571(7763), 90-94 (2019).
- [8] S. Singh, W. J. Jones, W. Siebrand *et al.*, “Laser Generation of Excitons and Fluorescence in Anthracene Crystals,” *J. Chem. Phys.*, 42(1), 330-342 (1965).
- [9] Y. J. Bae, G. Kang, C. D. Malliakas *et al.*, “Singlet Fission in 9,10-Bis(phenylethynyl)anthracene Thin Films,” *J. Am. Chem. Soc.*, 140(45), 15140-15144 (2018).
- [10] R. M. Young, S. C. Jensen, K. Edme *et al.*, “Ultrafast Two-Electron Transfer in a CdS Quantum Dot–Extended-Viologen Cyclophane Complex,” *J. Am. Chem. Soc.*, 138(19), 6163-6170 (2016).
- [11] S. W. Eaton, L. E. Shoer, S. D. Karlen *et al.*, “Singlet Exciton Fission in Polycrystalline Thin Films of a Slip-Stacked Perylenediimide,” *J. Am. Chem. Soc.*, 135(39), 14701-14712 (2013).
- [12] G. te Velde, F. M. Bickelhaupt, E. J. Baerends *et al.*, “Chemistry with ADF,” *J. Comp. Chem.*, 22(9), 931-967 (2001).
- [13] N. Renaud, P. A. Sherratt, and M. A. Ratner, “Mapping the relation between stacking geometries and singlet fission yield in a class of organic crystals,” *J. Phys. Chem. Lett.*, 4(7), 1065-1069 (2013).
- [14] M. Swart, and P. T. van Duijnen, “DRF90: a polarizable force field,” *Molec. Simul.*, 32(6), 471-484 (2006).
- [15] T. C. Berkelbach, M. S. Hybertsen, and D. R. Reichman, “Microscopic theory of singlet exciton fission. II. Application to pentacene dimers and the role of superexchange,” *J. Chem. Phys.*, 138(11), 114103 (2013).

- [16] E. A. Margulies, J. L. Logsdon, C. E. Miller *et al.*, “Direct Observation of a Charge-Transfer State Preceding High-Yield Singlet Fission in Terrylenediimide Thin Films,” *J. Am. Chem. Soc.*, 139(2), 663-671 (2017).
- [17] C. Grieco, G. S. Doucette, J. M. Munro *et al.*, “Triplet Transfer Mediates Triplet Pair Separation during Singlet Fission in 6,13-Bis(triisopropylsilylithynyl)-Pentacene,” *Adv. Funct. Mater.*, 27(46), 1703929 (2017).
- [18] P. E. Hartnett, E. A. Margulies, C. M. Mauck *et al.*, “Effects of Crystal Morphology on Singlet Exciton Fission in Diketopyrrolopyrrole Thin Films,” *J. Phys. Chem. B*, 120(7), 1357-1366 (2016).
- [19] M. Chen, Y. J. Bae, C. M. Mauck *et al.*, “Singlet Fission in Covalent Terrylenediimide Dimers: Probing the Nature of the Multiexciton State Using Femtosecond Mid-Infrared Spectroscopy,” *J. Am. Chem. Soc.*, 140(29), 9184-9192 (2018).
- [20] A. Mandal, M. Chen, E. D. Fosczcz *et al.*, “Two-Dimensional Electronic Spectroscopy Reveals Excitation Energy-Dependent State Mixing during Singlet Fission in a Terrylenediimide Dimer,” *J. Am. Chem. Soc.*, 140(51), 17907-17914 (2018).
- [21] K. Broch, J. Dieterle, F. Branchi *et al.*, “Robust singlet fission in pentacene thin films with tuned charge transfer interactions,” *Nat. Commun.*, 9(1), 954 (2018).